

COMPARISON OF TETRAHEDRAL AND HEXAHEDRAL MESHES FOR ORGAN FINITE ELEMENT MODELING: AN APPLICATION TO KIDNEY IMPACT

Xavier BOURDIN

INRETS - LBMC (UMR_T9406 INRETS/UCBL1), Bron, France

Xavier TROSSEILLE, Philippe PETIT

LAB PSA Peugeot-Citroen, Nanterre, France

Philippe BEILLAS

INRETS - LBMC (UMR_T9406 INRETS/UCBL1), Bron, France

Paper Number 07-0424

ABSTRACT

Hexahedral elements with a single integration point have been the solid elements of choice to represent organs in human finite element models for impact. While those elements have been known to be efficient in terms of stability and computational cost, they are difficult to generate and meshing represents a significant part of a model development time. The ever increasing level of details of biomechanical models further increases these meshing difficulties. In recent years, computing power has become affordable and new formulations of tetrahedral elements – that can be generated automatically even for complex shapes – have been introduced in the explicit finite element codes. The aim of this study was to evaluate the performance of two meshing approaches – semi-automatic hexahedron meshing vs. automatic tetrahedron meshing – for a simple biomechanical application. In this study, a kidney model was build based on the geometry from Visible Human Project dataset. Five types of 3D solid elements (8 node bricks with a single and 8 integration points, 20 node bricks, 4 and 10 node tetrahedrons) and two material laws (linear visco-elastic, hyperelastic viscous) were used to simulate a kidney blunt impact described in Schmitt and Snedeker [1].

While the drawbacks of tetrahedral elements were observed in particular in terms of computing cost, the difference in model response was found to be acceptable in a biomechanical characterized by large specimen to specimen variability. Furthermore, the tetrahedral element stability was found to be excellent.

For more complex shapes, the increased computing cost may be largely outweighed by the advantages of an automatic meshing approach.

INTRODUCTION

Hexahedral elements with a single integration point and hourglass control have been the elements of choice for human explicit finite element modeling.

Tetrahedral elements have rarely been used despite the fact that they are easy to create automatically while the generation of high quality hexahedral elements is very difficult for complex shapes such as those seen in the human body. One reason maybe that the hexahedral elements had important computing cost, stability and mechanical response advantages over the tetrahedral elements available in the past.

Human finite element models have become essential tools in automotive safety research. Besides numerous models of anatomical regions, several whole body human models are currently available (HUMOS2 from the HUMOS European consortium, THUMS from Toyota RD and the H-Model from ESI). However those models still need to be improved before they are able to reliably predict the risk of injury resulting from an impact. Future improvements may include:

- a more detailed description of the anatomical structures in order to better localize the injury prediction;
- better numerical stability and robustness;
- the consideration of specimen to specimen variations, both from geometrical and material properties standpoints.

Such developments are likely to make even more difficult the meshing, which is critical and very time consuming in human finite element modeling. For example in the case of the abdomen, if we compare the mesh of the HUMOS2 [2] model with a more detailed description of the abdominal anatomy derived from the Visible Human Project, it becomes apparent that further refinement will make the meshing task very difficult if the organs such as the intestines and their mesenteric attachment are simulated individually (Figure 1). The mesh quality - in terms of quality metrics such as the Jacobian, internal angles etc - resulting from such a complex mesh would likely be relatively poor, affecting in turn the stability of the model.

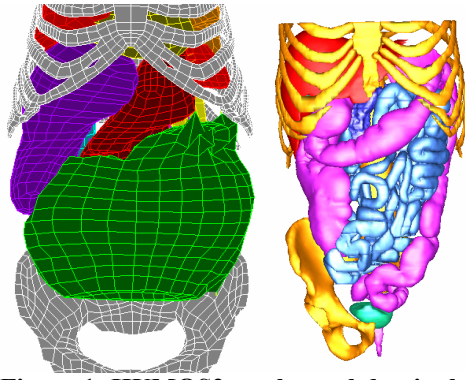


Figure 1: HUMOS2 mesh vs. abdominal geometry contoured at the L BMC (half of the pelvis only is displayed). Currently, the level of detail of HUMOS2 and of other finite element models of the abdomen does not allow simulating all organs individually.

Finally, the generation of different sets of meshes to take into account specimen to specimen variations would be time consuming even using scaling methods such as those used for the HUMOS2 model, as such methods are known to degrade the mesh quality, requiring manual corrections.

Those expected difficulties, associated with the availability of improved tetrahedral elements in the explicit codes and the development of low cost-high performance computing capability may make the drawbacks of tetrahedral elements acceptable, at least for research models. This can be evaluated by comparing simulation results using both approaches - tetrahedral and hexahedral meshing – while keeping all other modeling parameters identical (material properties, geometry etc).

This comparison was already made in the past for quasi-static simulations of the femur: Ramos and Simões [3] compared the results of 4-node and 10-node tetrahedral elements to 8-node and 20-node hexahedral elements and found the difference on the Von Mises stress predicted when loading the femoral head to be acceptable. While this is encouraging, these results obtained for hard tissues in an implicit code and quasi-static conditions are not necessarily applicable to soft tissues subjected to impact.

In this paper the use of tetrahedral element for soft tissues simulation during an impact were evaluated using a simple kidney model.

MATERIALS AND METHODS

Choice of loading condition

Schmitt and Snedeker [1] studied the biomechanical response of isolated kidneys

subjected to blunt impact. In their experiments, a pendulum was used to impact human (N=3) and porcine (N=65) kidneys. For the current study, the porcine dataset was selected because of its large number of specimen and because it provides tests results for various impact energies – from 1J to 6.08J – which are useful for the finite element model calibration. When comparing the human to the porcine kidneys results, the respective force versus displacement curves were of similar shape but slightly different amplitude. Based on their study, porcine and human kidneys are of similar geometrical shape and size.

Model generation: geometry and meshes

For the current study, a finite element model of the human kidney has been created based on the Visible Human Project dataset from the National Library of Medicine (Bethesda, MD). The image segmentation was performed manually using the IMOD (Univ. of Colorado, Boulder) software package in order to reconstruct a triangular surface representation of the organ. This surface was then scaled according to the geometrical average properties provided by Schmitt and Snedeker [1].

In order to simplify the problem and avoid a large number of numerical parameters, the kidney was assumed to be homogeneous and covered by a layer of shells representing the capsule covering the parenchyma. Two sets of meshes with similar number of elements were created using the ANSA software package (Beta-CAE, Thessaloniki, Greece): one hexahedral mesh with 1888 elements and one tetrahedral mesh with 1912 elements. The tetrahedral mesh was build automatically while the hexahedral mesh was build using surface to surface mapping. Those meshes were declined in five formulations of solid elements (Table 1) defined in the Radioss finite element code that was used for all simulations (Altair Engineering, Troy, MI). They were covered by 4-node shell or 3-node shell with coincident nodes on the outside surface.

Material properties

Two different types of material properties – hyper-elastic viscous (law 62 in Radioss) and linear visco-elastic (Bolzman law 34 in Radioss) – were used for the kidney.

Table 1. Elements used in the current study.

Simulation name	Element type
Brick8-1P	8 nodes brick, single integration point and hourglass control
Brick8-8P	8 node brick, 8 integration points
Brick20	20 nodes brick
Tetra4	4 nodes tetrahedron
Tetra10	10 nodes hexahedron

The law 62 is an hyper-elastic law where the strain energy function is given by:

$$W = \sum_{i=1}^n \frac{2\mu_i}{\alpha_i^2} \left(\lambda_1^{\alpha_i} + \lambda_2^{\alpha_i} + \lambda_3^{\alpha_i} - 3 + \frac{1}{\beta} (J^{-\alpha, \beta} - 1) \right),$$

where the λ_i are the principal stretches, J the volume variation and μ_i , α_i and β the material parameters. β can be defined using the Poisson ratio. The viscosity is modeled by a Prony series applied to all shear parameters.

The material parameters of the first order Mooney-Rivlin viscous material law (law17 in Pamcrash) used by Snedeker et al. [4] for the parenchyma in their model could not directly be used in this study because the respective formulations of the laws (62 in Radioss and 17 in Pamcrash) differ in the way the bulk response and the viscosity are handled. Furthermore, the current study makes the assumption that the kidney is homogenous while the study of Snedeker et al. [4] identified the properties of the parenchyma while a (softer) fluid component was simulated inside the kidney.

The material parameters used in the current study were therefore derived from the study of Snedeker et al. [4] properties as follows:

- an order $n=2$ was selected for the strain energy function, with $\alpha_1=2$ and $\alpha_2=-2$. This would be equivalent to a 1st order Mooney-Rivlin model in the case of incompressibility (see Appendix). In that case, if the Mooney Rivlin model used by Snedeker et al. [4] was transposed to this study, the constants μ_1 and μ_2 would be the double of their C_{01} , C_{10} constants (see Appendix): $\mu_1=410$ kPa and $\mu_2=363$ kPa respectively.
- a second order Prony series was used for the relaxation, keeping the same time constants as Snedeker et al. [4] (10 ms and 0.5 ms) and keeping similar ratio between the instantaneous and infinite moduli ($\gamma=G_\infty/G_0=0.6$ for the first time constant and $\gamma=G_\infty/G_0=0.35$ for the second time constant).
- A Poisson ratio of 0.47 was assumed in order to simulate the quasi-incompressibility of the solid
- The values of μ_1 and μ_2 were decreased by the same factor until a reasonable agreement was reached in terms of maximum displacement and maximum force in the 4.9J impact condition.

A similar approach was used for the linear visco-elastic law 34, keeping only one time constant (0.5 ms), and the same Poisson ratio (0.47). The

properties finally selected are summarized in the Tables 2 and 3.

It must be noted here that this approach does not aim to identify precisely material properties to use for the kidney subjected to blunt impact but only to be able to approximate the overall kidney response in order to compare the numerical performance of element types and laws.

For the capsule, the material properties were based on quasi-static experimental results by Snedeker et al. [5]. The capsule was assigned a thickness of 43 μ m and an elastic modulus of 15MPa as in their study. It was also assigned the same Poisson's ratio as the parenchyma (0.47) in the current study.

Other simulation parameters

The impactor and the wall were simulated with rigid bodies. The wall was fixed while the impactor was free to translate in the direction normal to the wall and was assigned an initial velocity. The contact between the kidney, wall and impactor were simulated using a bi-lateral surface to surface contact (type 7) in parallel with an edge to edge contact (type 11). A 0.05 friction coefficient was used for all contacts as used by Schmitt and Snedeker [1]. For the brick20 elements, all nodes – including the nodes located on the middle of the edges – were used in the contact interface with the impactor. In order to attach the shells of the kidney capsule to those nodes, a tied interface (type 2) was also defined. An overview of the simulation setup is provided Figure 2.

Simulation matrix

First, a parametric study with impact energies used by Schmitt and Snedeker [1] was performed in order to verify the ability of the selected material parameters to approximate the kidney impact response. The selected simulation matrix is available Table 4. This study was only performed using the brick8-1P elements.

Then, the 4.9J simulation was selected as the baseline condition and all types of elements were compared.

Finally, the impact velocity was increased until the model became unstable in order to test the tetra4 and brick8-1P elements ability to handle extreme conditions.

Table 2. Selection of material parameters for the law 62 used in the current study

Strain energy function parameters	Viscosity parameters (Prony series)
$\alpha_1=2$, $\mu_1=205$ kPa $\alpha_2=-2$, $\mu_2=181$ kPa $\nu=0.47$	$\tau_1=10$ ms, $\gamma_1=0.60$ $\tau_2=0.5$ ms, $\gamma_2=0.35$

Table 3. Selection of material parameters for the law 34 used in the current study.

$G_0 = 205 \text{ kPa}$ $\nu = 0.47$	$G_\infty = 82 \text{ kPa}$ $\tau = 0.5 \text{ ms}$
---	--

Table 4. Summary of impact conditions for the test of the material parameters

Velocity (m/s)	0.652	1.38	1.48	1.30	1.44	2.35
Impactor mass (kg)	4.7	2.2	2.2	4.7	4.7	2.2
Energy (J)	1	2.1	2.4	4.0	4.9	6.08

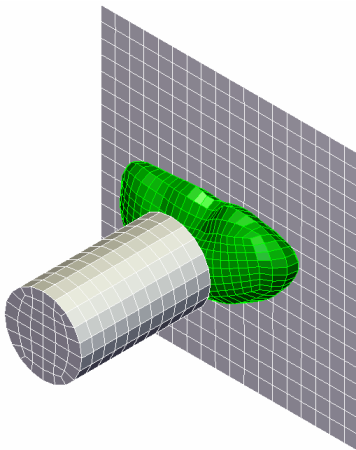


Figure 2. Overview of the simulation.

Comparison metrics

The model response was analyzed in terms of impactor force vs. impactor displacement curves, peak force and peak displacement, and energy dissipation. The force and displacement time histories were not available from the experimental studies and therefore could not be used to evaluate the models. The numerical behaviour was analyzed in terms of conservation of the energy balance, hourglass energy (when applicable), and time step conservation.

Regarding the computational cost, all simulations were run on the same machine (a dual Xeon EM64T at 3.06GHz) on two processors using the version 5.1d SMP Linux version. The machine was not running other jobs, and the user time, total time (sum of user and system time) were always within 1% of the wall clock time. The user time, number of time steps needed to finish the simulation and the cost per thousand cycles were used for the cost evaluation.

RESULTS

Comparison with the experimental data from Schmitt and Snedeker [1] at different energy levels (brick8-1P element only)

All the simulations performed with the brick8-1P element at energy levels between 1J and 6J ended with a normal termination, even for the highest energy case. Also, the hourglass remained within 10% of the energy of the simulation but there was a tendency for the hourglass to increase with impact energy, resulting in higher energy loss (from 3.2% at 1J, law 34 to 9.2% at 6J, law 62). Figure 3 shows a section of the mid-plane of the kidney at the peak impactor displacement for the 4.9J simulation. The force versus displacement response of the model was compared with the corresponding experimental results published by Schmitt and Snedeker [1] (Figure 4). Overall, the model response was similar to the experimental results, both in terms of peak force and peak displacement for all the energy levels with the exception of the 4J case. It must be noted that in the 4J test, the experimental peak force was between 650N and 850N, which is higher than the forces observed in the 4.9J test (between 600 and 735N). If comparing the responses of the laws 34 and 62, the two material models give very similar loading paths, peak force and peak displacement. However they differ significantly in unloading path and energy dissipation in the impact (area under the curve). The energy dissipation for the law 62 was 4.4J against 3.95 to 4.7J in the experiment. The energy dissipation for the law 34 was only 2.5J.

Comparison of the results for the different elements types at 4.9J

When testing the various element types, all simulations but two terminated normally. The law62 models using the brick8-8P and brick20 elements terminated with a negative volume after 19 ms and 32.4 ms respectively. All other simulations had energy balance errors lower than 6% at the end of the simulation (see Table 5, summary of the runs)

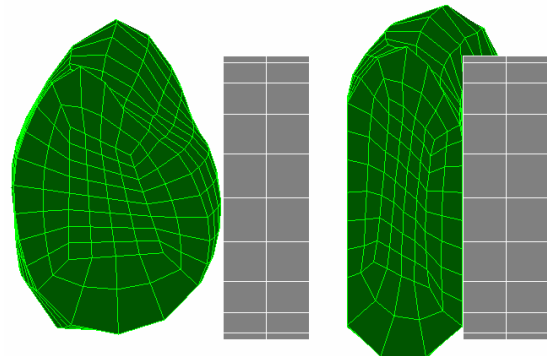


Figure 3. Mid section of the kidney at initial impactor position and peak impactor displacement for the 4.9J simulation.

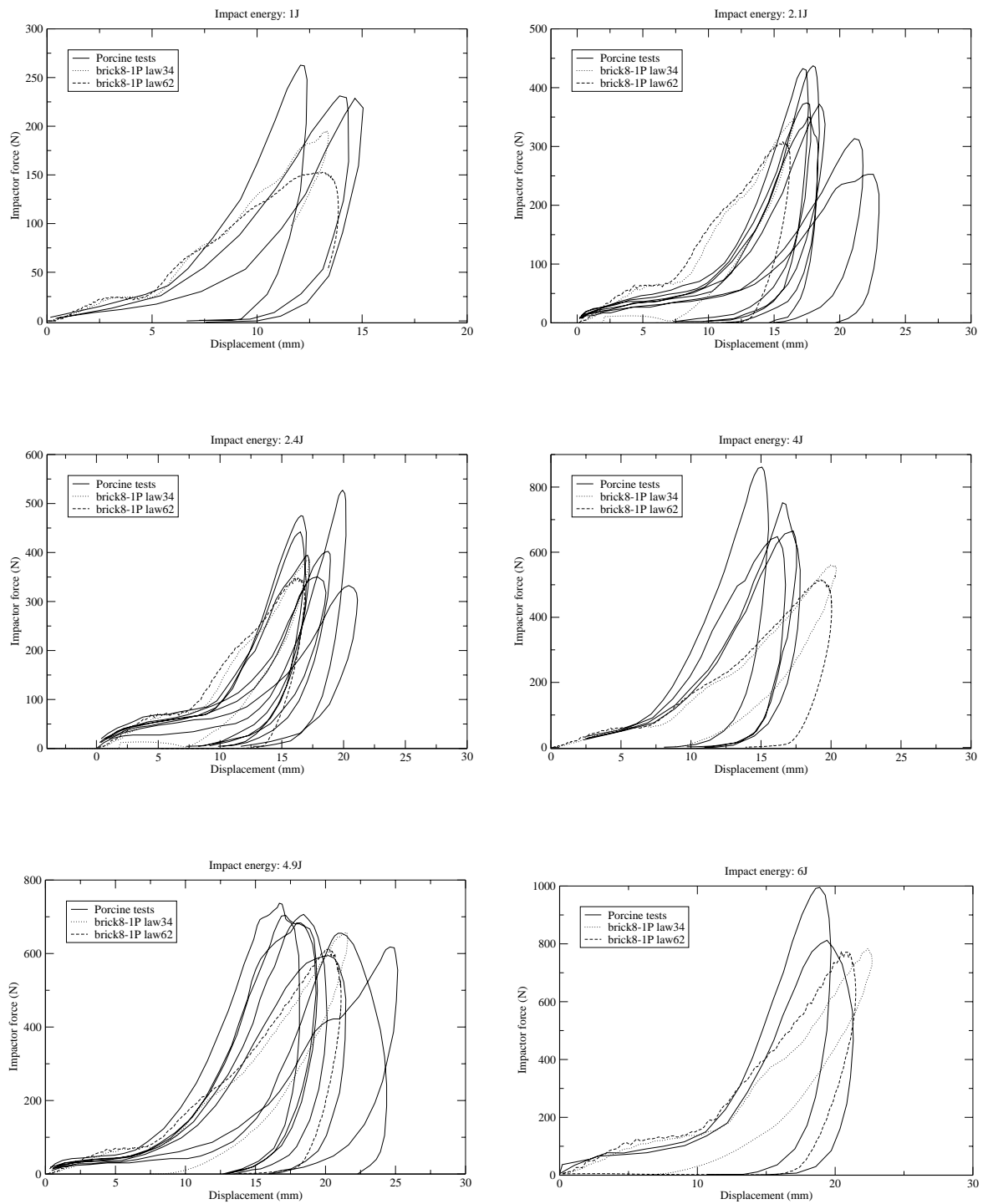


Figure 4. Comparison of the model response and the porcine test results for six impact energies from 1J to 6.08J. The solid lines represent typical tests results for each energy level.

Table 5. Summary of the runs

Elem.	Law	Term. Time(ms)	Error (%)	Total kCycles	Total User (s)	Time / kCycle	Av Tstep (μs)
brick8-1P	law62	40	-5.7	58	816	14	0.69
brick8-1P	law34	40	-6.7	59	367	6	0.68
tetra4	law62	40	-0.1	121	1427	12	0.33
tetra4	law34	40	-0.4	153	599	4	0.26
brick8-8P	law62	19.2	99.9	51	3848	75	0.39
brick8-8P	law34	40	-0.7	247	3125	13	0.16
tetra10	law62	40	-0.1	121	5025	41	0.33
tetra10	law34	40	-0.5	157	1606	10	0.26
brick20	law62	32.4	99.9	70	6563	93	0.46
brick20	law34	40	-0.4	283	8137	29	0.20

Where:

Termination time: number of ms simulated (40 for a normal termination)

Error (%): percentage of error in the energy balance at the end of the simulation

Total kCycle: total number of cycles run to reach the termination time divided by 1000

Total User (s): the computing time spent at the end of the simulation

Time / kcycle: the average computing time needed to run 1000 cycles

Av Tstep: average time step over the simulation

The force vs. displacement curves for all elements types and the law 62 are presented on Figure 5. After an initial non linear section (up to 7mm approximately) where the response of all elements is very similar, the force vs. displacement curves become more linear and differences between the element types appear. However, the difference between all element types is small when compared with the specimen to specimen variations. Also, for the given element density, the responses of the tetra4 vs tetra10 elements were almost identical. Similarly, the responses of the brick8-1P, brick20 and brick8-8P elements were very close until the computation terminated with an error for the brick8-8P. Overall; the tetra elements appeared stiffer than the brick8 elements with a 7% higher peak force and a 8% smaller peak displacement. The average stiffness was also calculated for each of the models in the region where the loading curves are almost linear (Figure 6). The tetra elements (48.5 N/mm) were approximately 14% stiffer than the brick8-1P elements (42.7 N/mm). Similar results were obtained for the law 34 (Figure 7). A summary of all stiffness results is provided Table 6. The stiffening for the tetra elements was lower than 10% (approx. 47 N/mm vs. 43 N/mm). The difference in peak force between tetra and brick was less than 6%, while the difference in peak displacement was less than 5%.

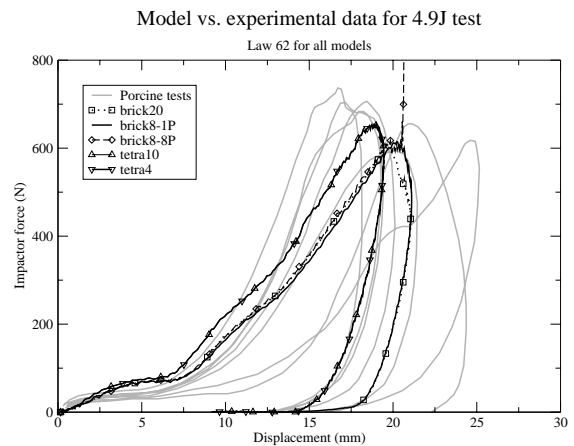


Figure 5. Force vs. displacement response for all elements types and the law 62 at 4.9J. The response of the 4 nodes and 10 nodes tetrahedron appears to be superimposed.

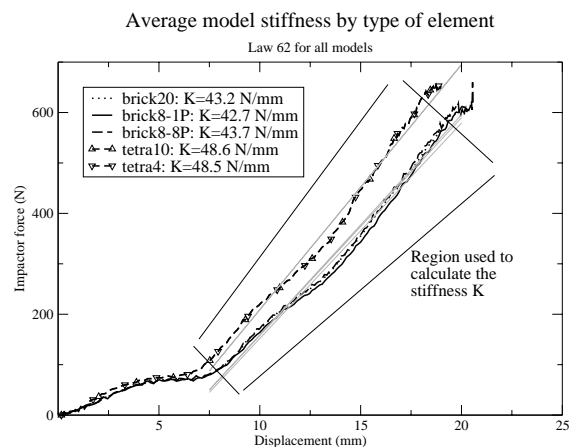


Figure 6. Stiffness calculation per element type. The stiffness was obtained by linear regression in the region plotted on the graph. The regression line obtained are plotted in light gray.

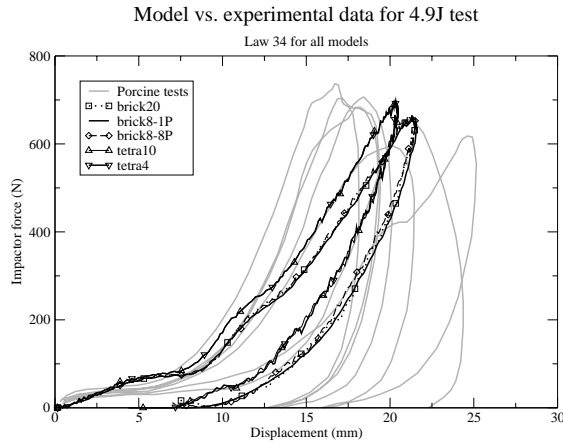


Figure 7. Force vs. displacement response for all elements types and the law 34 at 4.9J. The response of the 4 nodes and 10 nodes tetrahedron appears to be superimposed.

Table 6: Summary of stiffness depending on the element and the material law. All stiffness data are in N/mm

	brick20	brick8 1P	brick8 8P	tetra10	tetra4
Law34	43.1	42.9	43.4	47.0	47.0
Law62	47.6	42.7	43.7	48.6	48.5

Computing cost

There were large differences in computing time since they varied from approximately 5min (brick8-1P law34) to 2h26mn (brick20 law62) as described in Table 5. Multiple factors are responsible for those large variations, including:

- the material law, with the law 62 being 2 to 6 times more time consuming per cycle than the law 34;
- the type of element, with variations of up to 1 to over 6 on the cost per cycle (brick20 vs. tetra4) at identical material law;
- the average time step for the simulation, with variations of 1 to 4 approximately (that factor being also linked to the element type).

For a given material law, the tetra4 elements were faster than the brick8-1P if only the cost per cycle is considered, but the tetra4 models had a longer computational time since their average time step was lower.

Numerical Stability in extreme conditions (brick8-1P and tetra4 only)

When increasing incrementally the impact energy to 21.5J, the response of the brick8-1P and tetra4 elements was very different (Figure 8).

For the brick element, the hourglass energy increased rapidly with the impact velocity, resulting in a large loss in the energy balance: at 21.5J (4.7kg at 3m/s) with a law34, the simulation terminated

normally but the energy loss reached 48% (Figure 9). The deformation of the solid elements inside the mesh showed very large distortion in hourglass modes (Figure 10). The model with the law 62 terminated with error (Negative Volume) during the unloading phase at 21.05 ms of simulation time. The model terminated with error (Negative Volume) for higher impact energies.

For the tetra element, much higher energy levels could be reached (Figure 11) with a better energy balance without apparent abnormal element distortion (Figure 9). At 37.6J (4.7kg at 4m/s), the simulation terminated normally with an error of 2.6% on the energy balance for the law 62, and a 14.6% error for the law 34. When further increasing the impact energy to 58.7J (4.7kg at 5m/s), the model with the law 34 terminated with error (Negative Volume) at 11 ms at simulation time but the model with the law 62 terminated normally with only a 5.2% error on the energy balance (Figure 12).

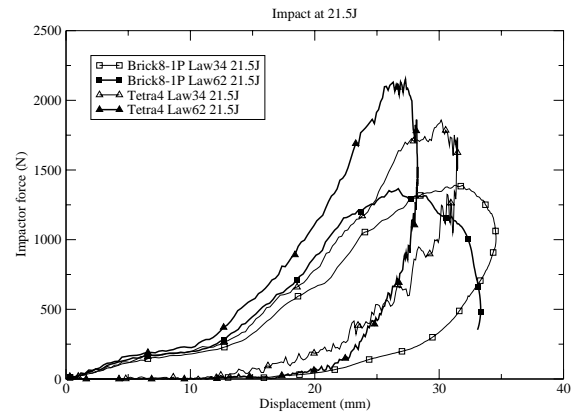


Figure 8. Force vs. displacement response for brick8-1P and tetra4 for laws 34 and 62 at 21.5J. The brick8-1P in law 62 terminated the simulation with an error during the unloading phase.

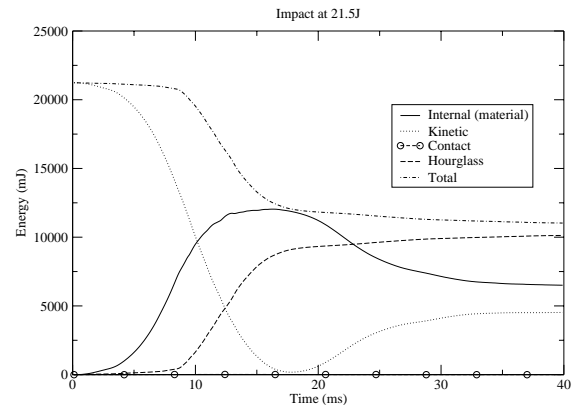


Figure 9. Energy vs. time response for hexahedron elements types and law34 at 21.5J.

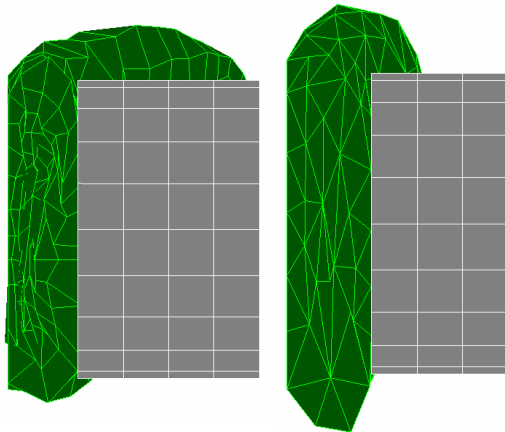


Figure 10. Examples of effect of extreme loading conditions on the model response: hexahedron elements for 21.5J at 16ms (left) and tetrahedron for 58.7J at 6ms (right)

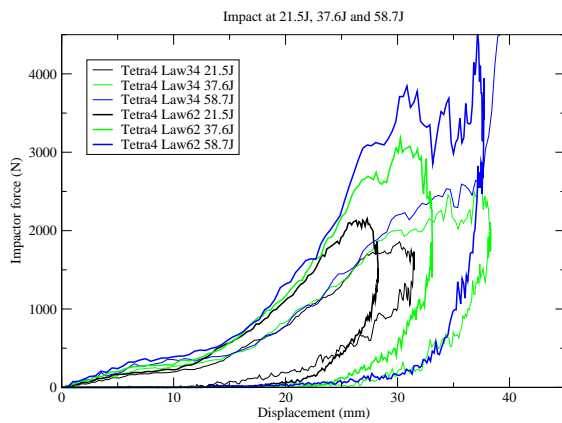


Figure 11. Force vs. displacement response for tetra4 elements and for laws 34 and 62 at 21.5J, 37.6J and 58.7J. The simulation terminated normally at 58.7J for the tetra4

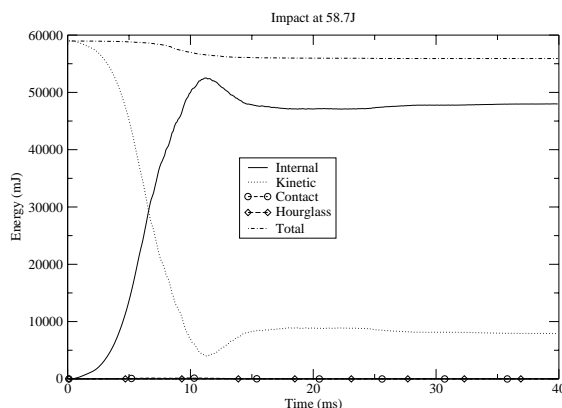


Figure 12. Energy vs. time response for tetrahedron elements types and law62 at 58.7J.

DISCUSSION

The material parameters used in the current study were identified by adapting properties proposed by Snedeker *et al.* [4] to approximate the overall response observed in the 4.9J experiments by Schmitt and Snedeker [1]. The laws selected were sufficient to approximate the overall response at other energy levels. There were larger discrepancies for some of the levels (4J in particular) but the comparison of the experimental results between different energy levels (4J vs. 4.9J) suggests that it may not be possible to match all the experimental responses with a single set of material properties or that other parameters that were not simulated have affected the testing results (positioning for example). While the material properties selected in this study may be inappropriate for other loading conditions, they are most likely sufficient for the current study which is only focusing on numerical aspects.

Both material models showed a fairly linear response after the initial loading where the non linear response may be due to contact non linearity and inertial loading. This phase of the response may be too linear when comparing it with the experimental data. A higher non linearity of the loading curve could be obtained by increasing the value of the α exponents in the hyperelastic viscous law but this is beyond the scope of this study. The main difference between the two laws is that the energy dissipation was lower for the law 34, which can be explained by the lack of the second time constant used in the law 62.

The effect of the number of integration points on the response was very limited: the brick20 and brick8-8P (fully integrated) were only marginally different from the brick8-1P element (with hourglass control) and the responses of tetra4 and tetra10 elements were virtually indistinguishable (Figures 5 and 7).

This result is of course very likely to change if the number of elements is decreased or if the loading mode is changed to include larger strain and stress gradients. A study on the effects of the mesh density would be useful. In the current application, a 1900 element model only represents a refinement lower than 3 of the HUMOS2 model which has approximately 100 elements as dividing the element size by 2 multiply their number by 8. In the current study, the mesh average element size was 5mm, and such a size may be needed to represent the complex anatomical structure of the abdomen.

When comparing the mechanical response of the various elements, the tetra (4 and 10 nodes) elements used in Radioss appeared to be 14% stiffer

(in the 4.9J case) than the brick8 elements. These differences are small when compared with the specimen to specimen variations and the uncertainties associated with the determination of material parameters.

In terms of stability, the brick8-8P and the brick20 were the only elements that did not terminate successfully the baseline level runs (4.9J). The detailed reason for the failure – and the possibility to stabilize the simulation – was not investigated as the interest of those elements with the current mesh density is very limited: they were at least 6 times as costly per cycle as the brick8-1P element but gave almost identical results. Similarly, the interest of the tetra10 is limited with the current mesh density as it did also provide virtually identical results as the tetra4 at a cost per cycle almost 4 times higher. Overall, this makes the brick8-1P and the tetra4 the two most interesting elements for the current mesh density.

When comparing the cost of the tetra4 and the brick8-1P, the lower time step of the tetra elements prevailed over its lower cost per cycle, resulting in a higher computing time (1.75 times higher in the case of the law 62).

Overall, this lower time step for the same average volume is the main drawback of the tetra4 element when compared with the 8 node brick element with a single integration point. In a larger model, this may be mitigated by the fact that the time step may not be determined by the soft tissues but by harder tissues like bone.

Regarding the stability of the brick8-1P elements, it must be noted that no effort was made to stabilize the simulations and it may be possible to further increase the brick stability in particular by changing numerical parameters such as the hourglass control formulation. Despite this and while using default options, both brick8-1P and tetra4 elements were stable for energies that were higher than the injurious energies proposed by Schmitt and Snedeker [6] (AIS = 5 for energies over 8J). This is a very encouraging result. For the conditions tested, the tetra element was much more stable than the brick, which had important hourglass problems. It was possible to reach very high compressions of the tetrahedral mesh, as the 58.7J simulation resulted in a compression of approximately 37.7mm while the initial thickness of kidney was 44mm. It is unclear if results obtained for such extreme deformations are realistic but the ability to terminate normally a simulation while respecting the energy balance is important when the complexity of a model increase and that the error termination of any of its components results in the failure of the simulation.

CONCLUSIONS

Simulations of the kidney subjected to blunt impact were conducted using an approximately 2000 element finite element model. Five element formulations and two material laws were tested. The model was able to approximate the kidney response to impacts of various energies ranging from 1 to 6J. For the element density selected, the number of integration points in the elements had little effect on the response. The tetrahedral elements appeared to be slightly stiffer than the hexahedral elements but the stiffness difference was limited to less than 14%. The tetrahedral elements were also more stable than the bricks when subjected to very high impact energies.

Overall for the current element size, the use of tetrahedral elements over 8 nodes bricks with a single integration point seems very promising. In the present study, their main drawback was their lower time step (at equivalent volume size) that led to higher computing cost (up to almost double). This would not be a significant drawback for research models considering the rapid evolutions of computing capability and the difficulty to generate hexahedral meshes for complex geometrical shapes.

Possible extensions of this evaluation could include the study of the effects of mesh density and complex in-situ loading on the model response.

REFERENCES

- [1] K.U. Schmitt and J.G. Snedeker. 2006. "Analysis of the biomechanical response of the kidney under blunt impact". *Traffic Injury Prevention*, 7:171–181.
- [2] P. Vezin and J.P. Verriest. 2005. "Development of a set of numerical human models for safety". *Proc. of the 19th Int. Tech. Conf. on the Enhanced Safety of Vehicles*. Paper 05-0163.
- [3] A. Ramos and J.A. Simões. 2006. "Tetrahedral versus hexahedral finite elements in numerical modelling of the proximal femur". *Technical note in Medical Engineering & Physics*, 28:916–924.
- [4] J.G. Snedeker et al. 2005. "Strain energy density as a rupture criterion for the kidney: impact tests on porcine organs, finite element simulation, and a baseline comparison between human and porcine tissues". *Journal of Biomechanics*, 38:993–1001
- [5] J.G. Snedeker et al. 2005. "Strain-rate dependent material properties of the porcine and human kidney capsule". *Journal of Biomechanics*, 38:1011–1021.

[6] K.U. Schmitt and J.G. Snedeker. 2006. “Kidney injury: an experimental investigation of blunt renal trauma”. *Journal of Trauma*, 60:880–884.

APPENDIX: Mooney Rivlin vs. Ogden formulations for the strain energy function in the case of incompressibility.

The Mooney Rivlin strain function is:

$$W = C_{01}(I_1 - 3) + C_{10}(I_2 - 3)$$

where: C_{01} , C_{10} are material constants. The invariants are:

$$I_1 = \lambda_1^2 + \lambda_2^2 + \lambda_3^2$$

$$I_2 = \lambda_1^2 \lambda_2^2 + \lambda_2^2 \lambda_3^2 + \lambda_1^2 \lambda_3^2$$

$$I_3 = \lambda_1^2 \lambda_2^2 \lambda_3^2 = 1$$

In the Ogden strain energy function:

$$W = \sum_{i=1}^n \frac{2\mu_i}{\alpha_i^2} (\lambda_1^{\alpha_i} + \lambda_2^{\alpha_i} + \lambda_3^{\alpha_i} - 3)$$

where the μ_i and α_i are the material constants and λ_i are the principal stretches. If using $n=2$, $\alpha_1=2$ and $\alpha_2=-2$, we obtain:

$$W = \frac{2\mu_1}{4}(I_1 - 3) + \frac{2\mu_2}{4}(I_2 - 3)$$

Finally: $\mu_1 = 2C_{01}$ and $\mu_2 = 2C_{10}$